S.Ye. Donets[1], V.V. Lytvynenko[1], O.A. Startsev[1], Yu.F. Lonin[2], A.G. Ponomarev[2], V.T. Uvarov[2]

Fractal analysis of fractograms of aluminum alloys irradiated with high current electron beam

[1]Institute of Electrophysics and Radiation Technologies, Kharkiv, 61002, Ukraine, vvlytvynenko@ukr.net
[2]NSC Kharkiv Institute of Physics and Technology, Kharkiv, 61108, Ukraine

The aluminum alloys D16 and AMg6 were irradiated using the high-current relativistic electron beam in vacuum. Intense electron irradiation of the materials modified their physical properties. The fractal character of the fracture surfaces' images was studied. The change of the fractality is a distinguished descriptor of the materials modification. The characteristic ductile and brittle fractures are accompanied with the change of the fractal dimension.

Keywords: aluminum alloy, fractal, electron beam, irradiation, modification.

Introduction

Obtaining protective surfaces is one of the key tasks for ensuring the safety of both human health and technical systems. Among the many existing approaches to tackle this problem for metals, the irradiation treatment of surfaces can be selected. The popular approaches in this domain are: (i) laser treatment, (ii) irradiation with ions, (iii) processing with electron beams. The focus of current research is on obtaining hardened surfaces of metal plates by irradiating them with high-current relativistic electron beams (HCEB). Relativistic energy of electrons provides a deeper influence into the material (a hundred microns at 0.3-0.5 MeV for light metals), while intensive currents induce extreme volumetric thermo-mechanical conditions [1,2]. This technology can be an efficient tool of modification of the metallic surface to the required performance characteristics: microhardness, abrasion resistance, corrosion resistance, etc. Also, they could be further combined with additional techniques like electro-erosive alloying to enhance the surface properties [3].

At the same time, it is known [2, 4] that the HCEB treatment has a heterogeneous impact on the metals due to its radiation, temperature, and shock-wave effects. In this case, the depth of the modified layer significantly exceeds the average range of electrons in the material. Thus, the microstructure together with such an indicator as the value of microhardness, change significantly along the depth. It is stipulated, that interlayers can dampen possible external impacts. It is also found that the pretreatment of aluminum alloys with HCEB leads to a significant improvement in their superplastic deformation [5]. The dislocation density distribution over the volume of the irradiated material and their spatial orientation change even more unpredictably. Considering the above list of effects that occur during the irradiation of HCEB metal plates from the point of view of the possibility of obtaining impact-resistant materials, we can say that they represent certain technological prospects. The protective property of the material depends on its ability to convert the kinetic energy of the striking object into its own internal energy, as well as into the energy of its own deformations in all directions, with the exception of the direction in which the protected object is located. It is possible to approach the implementation of such requirement by creating an anisotropy in the microstructure of a solid material utilizing HCEB.

Since we are dealing with a non-homogeneous distribution of the characteristics of an object, it is possible to use the apparatus of fractal analysis as a macro tool to

evaluate the effect the HCEB irradiation by examining the fractures of the irradiated materials and the reference material. The fractal analysis can provide quantitative descriptors of the objects under study. The relative change of those descriptors actually is a result of the change in the microstructures and their corresponding fracture mechanisms. A common fractal descriptor is a fractal dimension D. It denotes changes in complexity in the surface under study. The more complex is the surface (e.g., roughness, visible features), the more complex is the distribution of the fractal dimension [6]. However, one should be aware about that changes in D may not actually result in changes in particular mechanical properties and vice-versa as the techniques used to calculate D can be insensitive to the provided changes. For example, a hardness could change while a fractal dimension stays almost the same.

2 aluminum alloys were selected for study: AMg6 alloy of the Al-Mg system and D16 of the Al-Cu-Mg system. These alloys are commonly used in aerospace domain and for special light-vehicle production. These alloys were also studied by our team and results were presented in [7], and thus suited for this case study to investigate their fractures using fractal analyses.

I.   Materials and methods

The aluminum alloys D16 (91.9% Al; 4.8% Cu; 1.5% Mg; 0.8% Mn; impurities Fe and Si up to 0.5%, wt.%) and AMg6 (92.197% Al, 0.1% Cu; 6% Mg; 0.6% Mn; 0.4% Fe; 0.4% Si; 0.2% Zn; 0.1% Ti; 0.003% Be, wt.%) were used in the current research [7]. The samples of irradiated materials were prepared in a form suitable for subsequent mechanical deformations in various modes.

Irradiation was carried out on the TEMP-A pulsed electron accelerator NSC KIPT [1] with the current –2 kA, electron energy of 0.3 MeV, and the pulse duration around 5 µs. The irradiation was conducted in the vacuum.

To prepare the samples for fractographic analyses, the samples were broken at a room temperature and the fractures were studied using a JEOL JSM-840 scanning electron microscope.

Fractal character of the SEM images of fractures was studied as per methodology described in [8]. Variation of intensity in the grayscale SEM images of microstructures is a composite characteristic property which depends on the fracture roughness, grain structure, and on the scanning properties such as illumination (signal) and focus. If it may be assumed that the microscope imaging conditions are optimal, then the fractal analysis can be performed for the SEM images to describe the target microstructures.

Fractal dimension analyses were conducted using the in-house software package based on the Clarke's triangular prism surface area method (TPSAM) and spin-off methods [9, 10]. Basically, Clarke extended the Mandelbrot approach to an area grid. TPSAM enables calculation of the fractal dimension of a digital surface by plotting virtual prisms on the surface using the pixel gray-level values. The surface area A is covered with the triangular prisms on a square window with a step size δ. Then, a least square regression of A-δ though the data

points is plotted for multiple δ on the log-log scale [11]:

$$A(\delta) = N(\delta)\delta^2 = K\delta^{2-D} \qquad (1)$$

$$Log(A) = K + (2 - D)Log(\delta) \qquad (2)$$

$$D = 2 - \beta \qquad (3)$$

where $N(\delta)$ is a number of steps performed, K is a constant, D is a fractal dimension, while β is a slope of the regression line. If there is no slope of the line $log(D)$-$log(\delta)$, then D tends to the theoretical value of 2. In other terms, a grayscale image is considered as a matrix of certain $x \times y$ pixel size, while a gray-scale intensity (1..256) of an image is considered as a height. Thus, it is possible to cover the image with virtual prisms and calculate a fractal dimension map as described above.

The corresponding software package was previously developed in Pascal/Delphi [12]. For calculations in this research, the original TPSAM method was selected on the squared windows 4x4 pixels with a sliding step of 1 px. The data A-δ was calculated increasing the step size δ from 1 to 4 px. A starting point for a 1 px prism was taken as a top left corner of an image, selection of such starting point was assumed to have a negligible effect as the calculation was done with a sliding step of 1 px in x & y directions. Next, a slope of a regression line was calculated. Small window size minimized blurring and smoothing of the features. TPSAM method is known to underestimate or distort the fractal dimension D, thus the tests were conducted to establish such effects. In general, the possible over- or underestimations of the fractal dimension are of less importance because the fractal analyses are used for comparison between samples, and in the case if we need to make a correction for the underestimation, it is advised to refer to the study in [13]. Regarding error of calculations of fractal dimensions, it is possible to estimate it directly from computations, however, it makes the computations more complex, and it is harder to relate to them. It was recommended to do actual tests on images, if a fractal dimension tends to some theoretical expected value. The authors followed the latter approach.

The necessary visualizations and data post-processing were performed in Python 3, incl. the library plotly v5.11. The scripts were written in the Jupyter notebooks which facilitates development due to user friendliness and collaboration between the developers.

II. Discussion

Prior to analyses, the tests of fractal calculations were performed. As the data objects for analyses are SEM images, it was necessary to establish how the algorithm calculate the fractal dimension D for some simple cases. For example, Fig. 1a shows the test sample 1 which is a cropped piece of the SEM image of the relatively flat fracture surface and the test sample 2 which is also a piece of SEM image but out-of-focus sample surface. The sample 1 was actually taken from Fig. 2b and the sample 2 was from Fig. 2a. Having calculated the fractal dimensions, the fractal maps were obtained. As the

sampling window was 4x4 pixels, the actual smoothing effect was not large compared to the cases with large sampling windows like 10x10. However, as the algorithm slides across 2 dimensions of the SEM image while processing the grayscale intensity, some blurring appears. The blurring effect is noticeable on the sharp boundaries. For example, the sample 1 has a white background due to cropping. This boundary blurs on the fractal map. Thus, it is important to have high-resolution images and to minimize a sampling window size while trying to explore small objects with higher accuracy.

When the fractal maps are calculated, one can plot a distribution of fractal dimensions against number of pixels. Such fractal distributions are presented on Fig. 1b, but they are also normalized on the maximum value of frequency of pixels in each distribution to enable relative comparison between the samples. The bin size of fractal dimension for all our distributions is 0.01. The sharp peak at $D{\sim}2$ for the sample 1 corresponds to the white background of the cropped image. Basically, a flat 2-dimensional surface should have no features and no complexity. When the pixel intensities start to variate, D grows. The flat fracture surface of the sample 1 has a second peak at $D{\sim}2.37$. The sample 2 has a wide peak at 2.46, which is characterizes a more chaotic object. It

appears, that the method is sensitive to the small variations of intensities or noise as expected [10]. Noisier SEM images will have a wider peak at $D{\sim}2.5$. It is seen that the calculated value at the peak $D{\sim}2$, tends to the theoretical value at $D{\sim}2$. A calculation error can be estimated as a full width at a half maximum, and it was around ~ 0.01 (however, for that particular test a bin size for a fractal dimension distribution was taken at 0.002). The relative error of all calculations of fractal dimensions in this research was assumed to be around ~ 0.01.

During calculations of D, the actual values are not limited within a max theoretical value of 3 and a min value of 2. The Clarke's algorithm may not fit properly the actual surface with the virtual prisms, thus, leaving for some errors. So, the values might be a little lower than 2 or higher than 3 for few points on the large SEM image. With those assumptions, it is now possible to proceed to analyses of the real fractograms.

Fig. 2 shows the fractogram of the AMg6 alloy. On the left side of Fig. 2a, the target surface is melted by the beam, which is characterized by grain elongated perpendicular to the surface. This is a common recrystallized microstructure of the melted zone (MZ) due to directional crystallization. The thickness of the recrystallized MZ reaches ~ 100 µm at the epicenter of
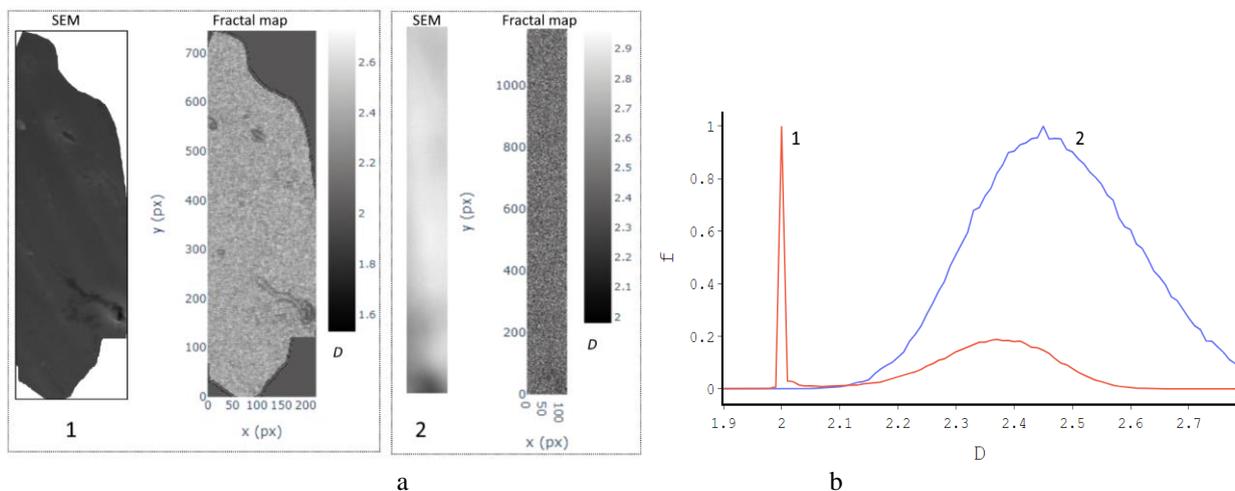
Fig. 1. Tests on pieces of SEM images (a) and their corresponding (b) distribution of the normalized frequency of the calculated fractal dimensions of the SEM images, where (1) is the test sample 1, (2) is the test sample 2.
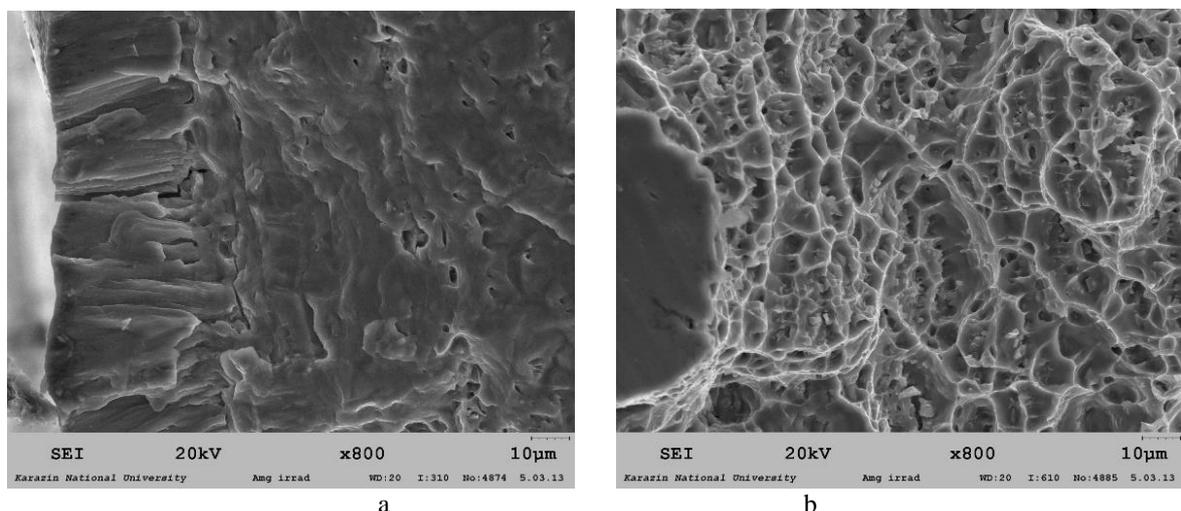
Fig. 2. Fractograms of the fracture of the AMg6 alloy. (a) irradiated material, near-surface area, (b) reference material in the central part of the sample

irradiation, however, the beam melts up to the depth of around 500-600 µm but most of the material is lost due to ablation into the environment. The elongated grains have a thickness of ~1-5 µm, and traversing the whole MZ. On the right side of Fig. 2a, there is a rough globular microstructure. This is a heat-affected zone (HAZ), which was impacted by the thermal and shock-wave effects of the beam. The microhardness of such irradiated area is 20% higher compared to the reference material as reported elsewhere [7]. Apart from recrystallization effects, the formation of compression-tension waves in the target volume contributes to the change of microstructure as it was discussed in [14]. The fracture mechanism of MZ is brittle with clear intercrystalline cracks and between MZ and HAZ. In the latter case, the cracks appeared confirming a poor adhesion between the recrystallized layer and HAZ base, Fig. 2a.

Fig. 2b shows a fragment of the central part of the plate. This part was not affected by the HCEB irradiation and it represents the reference material. The reference alloy AMg6 has the faceted microstructure of a size 2-8 µm. Its fracture mechanism is of predominantly ductile mode with elements of brittle fracture. There are many fine independent dimples with a diameter ~2 µm, uniformly distributed across the fractogram. Presence of hardening phase in terms of small particles with a size 0.5-3 µm was noticed on the facet boundaries. It is assumed that those are Al_2Mg_3, $(Fe, Mn)A_{l6}$, Mg_2Si as found in

[15].

In general, the HCEB irradiation resulted in formation of the thin brittle surface layer of recrystallized material. The mechanical properties at MZ deteriorated in terms as a protective layer. It is known, that HCEB processing of the materials results in some residual compressive stresses, which actually lead to lower adhesion of the melted zone of material to the bulk material. The stresses were estimated to reach around 80-150 MPa [16].
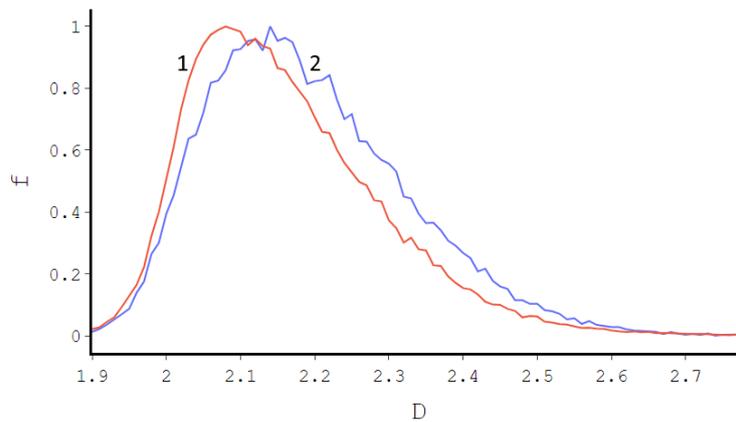
The fractal dimension maps of the SEM images on Fig. 2, are presented on Fig. 3a-b. The gray scale color bar is characteristic similar for both, and it is omitted for Fig. 3b. It is seen, the fractal analysis is a powerful tool for edge detection. It clearly highlighted the grain boundaries and the fracture cracks as the dark features which are visible on the gray 'noise' background. The normalized frequency distributions revealed the differences in the fractal dimension for the MZ, HAZ and the reference material. It appeared, the faceted microstructure of the reference material has a larger contribution of the edge boundaries, thus leading to a shift to lower D values. The melted zone itself has the highest contribution of the background noise as it is featureless compared to others judging on its peak position and width with trails. HAZ with the faceted-globular microstructure has intermediate distribution of fractal dimensions due to its nature of formation. To illustrate the difference between 'noise' background and the edge features, Fig. 3d was built by

a

b

c

d
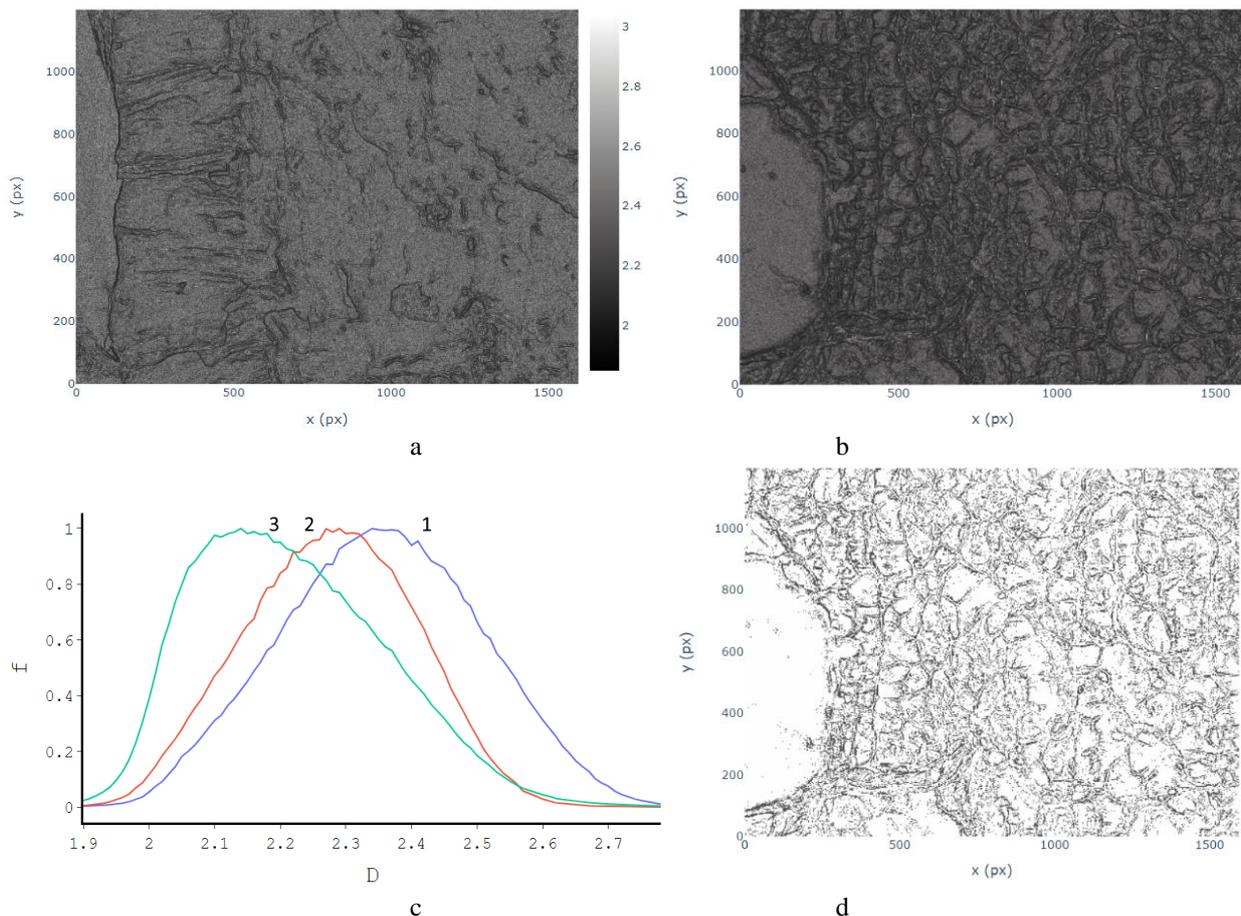
Fig. 3. Calculated fractal dimensions of the SEM images for the AMg6 alloy: (a) irradiated material, (b) reference non-irradiated material. The color bar of the fractal dimension D is included in (a) for illustrative purposes. (c) shows the distribution of the normalized frequency in the areas: 1) MZ, 2) HAZ, 3) non-irradiated reference. (d) illustrates a filtered fractal dimension map for (b), where $D < 2.2$.
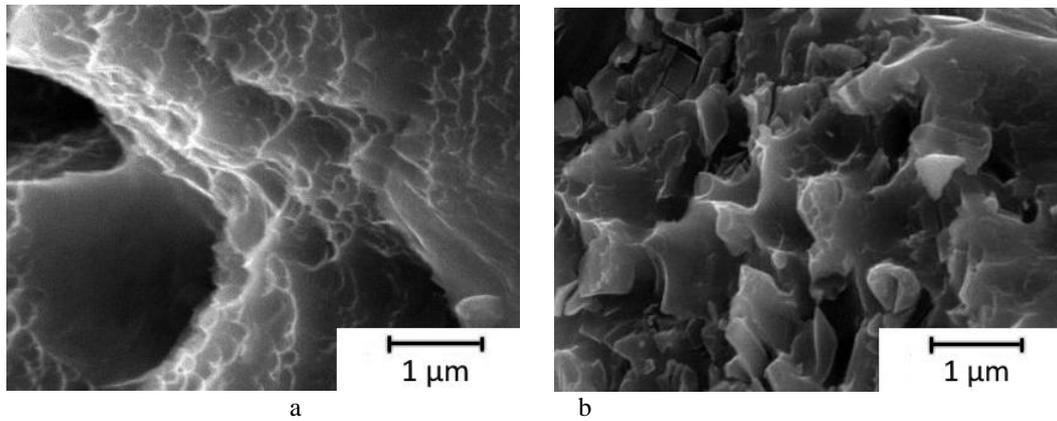
Fig. 4. Fractograms of the D16 alloy: a) irradiated (HAZ) zone, b) non-irradiated reference.

Fig. 5. Distribution of the normalized frequency of the calculated fractal dimensions of the SEM images in the areas: 1) irradiated (HAZ) zone, 2) non-irradiated reference of the D16 alloy.

filtering the Fig. 3b data set for $D < 2.2$. Some differences between the backgrounds ($D>2.2$) for all zones can be found, but it is currently unclear what is an actual effect of the SEM imaging conditions and the actual microstructures, and it requires some future investigations.

The study of the fractures of the D16 aluminum alloy were started earlier by the team in [7]. As it can be seen in Fig. 4a, the fracture of the irradiated part of the target was accompanied by the release of internal stress energy, which manifested itself in the deformation at the mesoscale level. The reference material is presented on Fig. 4b, the fracture went in a predominantly brittle mode with intergranular fracture and fine dimples. The irradiated material has the ductile mechanism of fracture in the heat-affected zone, accompanied with large deep dimples and tear ridges. From the point of view of absorption of external shock energy, the irradiated material may be better as a protection layer. Fractal dimension analyses (Fig. 5) revealed the shift of the distribution to lower D values, both in terms of a peak position and a higher-D trail. The shift in the fractal dimension distribution is basically contributed by the change in the fracture mode and thus, in a presence of more edge features. Based on the results from the AMg6 alloy and the D16 alloy, it appeared that the more brittle aluminum alloys are, the higher is the contribution of noise, and the higher ductile microstructures have the SEM fractograms with the distributions significantly contributing at $D\sim2$.

It is suggested, that the nonlinearity of the behavior of the mechanical properties of the aluminum alloys can be extended by considering the fractal dimension of the microstructure, i.e. their fractures. In such case, the behavior may follow the modified Hall-Petch expression as described by Tian et al. in [17]:

$$\sigma = \frac{F}{A}\left(1 + \frac{k}{r^{2\alpha-2}}\right) \qquad (4)$$

where F is the applied force to the crystalline object with a section of size A, k is a constant, r is a size of crystallites or grains, and α is a fractal dimension. It becomes the classic Hall-Petch relationship when $\alpha=5/4$. In general, it is hypothesized, that the fractal dimension influences on the local mechanical properties, and it could be useful to do tensile testing, or pico- or nano-hardness testing in future to confirm the relation. Also, more solid understanding of the fractal descriptors of the fractures and the microstructure, could assist with prediction of materials failure. However, it is still unclear how the calculated fractal dimensions should be used as the distributions have large contribution of noise, chaotic variations of SEM imaging conditions. A possible improvement is extraction of components from the fractal dimension distributions as on Fig. 3: noise/background as a gaussian distribution with a peak around $D\sim2.4$-2.5, and contribution of other features with peaks at $D\sim2$-2.3. More studies are planned to be conducted in this field by our team.

253

The possible application domains of fractal analyses of microstructure images could be extended to more simple matters as it simplifies the edge detection for the grain boundaries and other high-contrast features. For example, the automated analyses of microstructure can be implemented if combined with other methods. Such approach may provide the details on the fracture mechanisms, comparisons of microstructures, quantitative description of the microstructures.

Conclusions

Modification of the surfaces of aluminum alloys by processing with high-current relativistic electron beams changes the microstructural nature of their near-surface layer. HCEB processing of the AMg6 alloy caused embrittlement of the melted area. The heat-affected zone of the materials also went through substantial changes in microstructure. HAZ in D16 alloy became more ductile compared to the reference material. The fractal analyses revealed the distinct differences of the alloys before and after modification in terms of fractal dimension of the SEM images of their fracture surfaces. More ductile sample areas appeared to have a larger contribution of fractal dimension close to 2, compared to more brittle microstructures due to abundance of edge features in the former case.

Donets S.Ye. – PhD, Senior Scientist Research Fellow, Institute of Electrophysics & Radiation Technologies National Academy of Sciences of Ukraine;
Lytvynenko V.V. – Dr. Tech. Sc., Director, Institute of Electrophysics & Radiation Technologies, National Academy of Sciences of Ukraine;
Startsev O.A. – PhD, Research Fellow, Institute of Electrophysics & Radiation Technologies, National Academy of Sciences of Ukraine;
Lonin Yu.F. – Dr. Tech. Sc., Head of Department, NSC Kharkiv Institute of Physics and Technology National Academy of Sciences of Ukraine;
Ponomarev A.G. – PhD, Head of Laboratory, NSC Kharkiv Institute of Physics and Technology National Academy of Sciences of Ukraine;
Uvarov V.T. – PhD, Senior Scientist, NSC Kharkiv Institute of Physics and Technology National Academy of Sciences of Ukraine.

[1] V.T. Uvarov et al., *Radiation acoustic control over the thermal parameter of construction materials irradiated by intense relativistic electron beam*. Physics of Particles and Nuclei Letters. 11(3) (2014); https://doi.org/10.1134/S1547477114030157.

[2] V.V. Bryukhovetsky et al., *The structural phase state and strength properties of the surface layer of AA6111-T4 aluminum alloy irradiated by the high-current electron beam*, Nuclear Instruments and Methods in Physics Research, Section B: Beam Interactions with Materials and Atoms, 519 (2022); https://doi.org/10.1016/j.nimb.2022.03.008.

[3] V. Tarelnyk et al., *New sulphiding method for steel and cast iron parts*, IOP Conference Series: Materials Science and Engineering, 233(1), 012049; https://doi.org/10.1088/1757-899X/233/1/012049.

[4] V.V. Bryukhovetsky et al., *The features of the structural state and phase composition of the surface layer of aluminum alloy Al-Mg-Cu-Zn-Zr irradiated by the high current electron beam*, Nuclear Instruments and Methods in Physics Research, Section B: Beam Interactions with Materials and Atoms, 499 (2021); https://doi.org/10.1016/j.nimb.2021.02.011.

[5] V. V. Bryukhovetskii et al., *Effect of pulsed electron irradiation on the parameters of duraluminum superplasticity*, Fiz. Khim. Obrab. Mater., 4 (2002); https://www.researchgate.net/publication/292062571_Effect_of_the_pulsed_electron_irradiation_on_superplasticity_properties_of_duraluminum.

[6] M. Tarafder et al., *Fractal analysis of microstructural images for evaluation of HSLA steel*. Supplemental Proceeding, TMS, 2 (2010); https://eprints.nmlindia.org/3309/.

[7] M.I. Bazaleev et al., *Aluminum alloys shock protective surfaces modified by high current electron beam*, Journal of Surface Physics and Engineering, 1 (2017); http://dspace.nbuv.gov.ua/handle/123456789/122608.

[8] V.F. Klepikov et al., *Fractality of Fractures of Aluminum and Titanium Alloys Irradiated by Intensive Electron Beam*, Journal of Nano- and Electronic Physics, 8(3) 03009 (2016); https://doi.org/ 10.21272/jnep.8(3).03009.

[9] K.C. Clarke, *Computation of the fractal dimension of topographic surfaces using the triangular prism surface area method*, Computers & Geosciences, 12(5) (1986); https://doi.org/10.1016/0098-3004(86)90047-6.

[10] W. Sun et al., *Three New Implementations of the Triangular Prism Method for Computing the Fractal Dimension of Remote Sensing Images*. Photogrammetric Engineering and Remote Sensing, 72(4) (2006); https://doi.org/10.1080/01431160600676695.

[11] C. Nayak, *Comparing various fractal models for analyzing vegetation cover types at different resolutions with the change in altitude and season*, MSc Thesis, ITC, IIRS (2008); https://webapps.itc.utwente.nl/librarywww/papers_2008/msc/gfm/nayak.pdf.

[12] A. Startsev, *Calculation of fractal maps for data sets*, IERT NAS of Ukraine (2014); https://github.com/oleksandrstartsev/FractalsDimPRGs.

[13] M.K. Rathore et al., *Estimation of Fractal Dimension of Digital Images*, International Journal of Engineering and Technical Research (IJETR), 2(9) (2014); https://www.erpublication.org/published_paper/IJETR022497.pdf.

[14] V.V. Bryukhovetskii et al., *Features of gelation of surface of industrial aluminium alloy 6111 in the area of influence of impulsive bunch of electrons in the mode of pre-melting*, Problems of Atomic Science and Technology, 72(2) (2011); https://vant.kipt.kharkov.ua/ARTICLE/VANT_2011_2/article_2011_2_28.pdf.

[15] G.I. Prokopenko et al., *Hardening of Surface Layer on Al—6Mg Aluminium Alloy, Using Complex Effects of Electric Spark and Ultrasonic Impact Treatments*, Metallofiz. Noveishie Tekhnol. 35(10) (2013).

[16] V.F. Klepikov et al., *Physical and mechanical properties of titanium alloy VT1-0 after high-current electron beam irradiation,* Problems of Atomic Science and Technology 96(2) (2015); https://vant.kipt.kharkov.ua/ARTICLE/VANT_2015_2/article_2015_2_39.pdf.

[17] Dan Tian et al. *Hall–Petch effect and inverse Hall–Petch effect: a fractal unification*, Fractals, 26(06) (2018); https://doi.org/10.1142/S0218348X18500834.

С.Є. Донець[1], В.В. Литвиненко[1], О.А. Старцев[1], Ю.Ф. Лонін[2], А.Г. Пономарьов[2], В.Т. Уваров[2]

Фрактальний аналіз фрактограм алюмінієвих сплавів, модифікованих сильнострумовим електронним пучком

[1]*Інститут електрофізики та радіаційних технологій, м. Харків, 61002, Україна, vvlytvynenko@ukr.net*
[2]*ННЦ Харківський фізико-технічний інститут, м. Харків, 61108, Україна*

Алюмінієві сплави Д16 і АМг6 опромінено сильнострумовим релятивістським електронним пучком у вакуумі. Інтенсивне електронне опромінення матеріалів зумовило зміну фізичних властивостей сплавів. Досліджено фрактальний характер зображень поверхонь зламів. Зміна фрактальності є відмінним параметром опису модифікації матеріалів. Характерні пластичні та крихкі руйнування супроводжуються зміною розподілу фрактальної розмірності.

Ключові слова: алюмінієвий сплав, фрактал, електронний пучок, опромінення, модифікація.